International Journal of Heat and Mass Transfer 52 (2009) 1023–1035

Contents lists available at ScienceDirect

International Journal of Heat and Mass Transfer

journal homepage: www.elsevier.com/locate/ijhmt

Numerical study of mixed convection in a two-dimensional laminar incompressible offset jet flow

K. Kumar Raja [a,1], Manab Kumar Das [a,*,2], P. Rajesh Kanna [b]

[a] Department of Mechanical Engineering, Indian Institute of Technology Guwahati, North Guwahati-781 039, India
[b] Department of Mechanical Engineering, Kalasalingam University, Krishnan Koil-626 196, India

ARTICLE INFO

Article history:
Received 13 February 2007
Received in revised form 7 July 2008
Available online 26 September 2008

Keywords:
Offset jet
Mixed convection
Computation

ABSTRACT

The mixed convection flow and heat transfer characteristics in a two-dimensional plane, laminar offset jet issuing parallel to an isothermal flat plate have been investigated numerically. The unsteady form of the vorticity transport equation has been solved to obtain the steady-state solution. The isothermal heated plate is 30 times the jet width and the offset ratio is 1. The behavior of the jet in the range of Reynolds number $Re = 300–600$ and Grashof number $Gr = 10^3–10^7$ is described in details. The medium considered is air ($Pr = 0.71$). It is found that the reattachment length is strongly dependent on both Re and Gr for the range considered. Simulations are made to show the effect of entrainment on the recirculation eddy. The variation of the local Nusselt number is presented for various Re and Gr. An empirical correlation of average Nusselt number as a function of Richardson number ($Ri = Gr/Re^2$) and Re has been given.

1. Introduction

Mixed convection flow arises due to the buoyancy forces in addition to the forced convection flows. Mixed convection flow is encountered in many industrial situations. This kind of situation is encountered in electronics cooling, defroster system, paper industry fluid injection systems, heat exchangers, cooling of combustion chamber wall in a gas turbine, automobile demister and others.

The flow field of an offset jet is complex and is found in many engineering applications. For instances, burners, boilers, gas turbine combustion chambers, and fuel injection systems are strongly governed by the behavior of offset jets. Fundamental study of the flow field of offset jets can also lead to better understanding of similar flows such as backward-facing step flows and sudden expansion flows. A jet can be analyzed as a free jet or bounded one, depending on distances form the discharge to the confining boundaries. If the boundaries are sufficiently far from the discharge, the flow can be considered as a free jet. However, a bounded jet will occur when it interacts with a parallel wall. Bounded jets can be classified into three types: (a) an impinging jet aimed toward the boundary; (b) a wall jet where the fluid is discharged at the boundary; and (c) an offset jet from a vertical wall of a stagnant pool issuing parallel to a horizontal solid wall.

The flow emanating from a two-dimensional (2D) offset jet is shown in Fig. 1(a) where the main features and regions of interest are depicted. Fluid is discharged from a slot inside a wall into the ambient near a solid boundary parallel to the inlet jet direction. Due to the entrainment of fluid between the jet and the plate, there is a reduction of pressure in this region forcing the jet to deflect towards the boundary and eventually attach with it. This is called the Coanda effect [1]. The offset jet behaves differently in various regions. In the near field within a very short distance from the point of discharge, the jet is momentum dominated flow having the properties of free jet. Attachment may occur when the jet is deflected by an adjacent solid wall or a free surface and tends to flow along the boundary. In the region around attachment point, that is, the impingement region and part of preattachment region, the jet has the characteristics an impingement jet. The jet becomes a wall jet in the downstream far field. The other factors such as ambient motion (free-stream velocity), buoyancy (density difference), discharge orientation, etc. further complicate the jet-boundary interaction and the behavior of an offset jet. When the density of the discharged fluid is different from that of the ambient fluid, a buoyant jet is formed and driven to rise up or fall down by a buoyant force. When the buoyant force acts in the opposite direction of the main fluid flow, it is called buoyancy opposing flow.

In the other case it is called buoyancy aiding flow. Buoyancy opposing flow has been studied by Higuera [2]. The behavior of a buoyant offset jet is governed by buoyancy force and stratification as well as boundaries. Cheng et al. [3] have presented a numerical study of the buoyancy effect on the flow and heat transfer in an

* Corresponding author.
E-mail addresses: komarala1@gmail.com (K.K. Raja), manab@mech.iitkgp.ernet.in (M.K. Das), prkanna@gmail.com (P.R. Kanna).
[1] Present address: Emp No: 57205, EG72 Project. The CAPITAL, Polaris Software Labs Limited, Gachhibowli, Hyderabad, India.
[2] Present address: Associate Professor, Department of Mechanical Engineering, Indian Institute of Technology Kharagpur, West Bengal, 721302, India.

0017-9310/$ - see front matter © 2008 Elsevier Ltd. All rights reserved.
doi:10.1016/j.ijheatmasstransfer.2008.07.033

Nomenclature

g	gravitational acceleration, m/s^2
Gr	Grashoff's number, $\left(\frac{L^3 g\beta\Delta T}{\nu^2}\right)$
h	inlet slot height, m
H	offset height
i	x-direction grid point
j	y-direction grid point
L	length of the plate, m
Nu	local Nusselt number, $-\partial\theta/\partial y$
$\overline{Nu}$	average Nusselt number
n	normal direction
Pr	Prandtl number, $\frac{\nu}{\alpha}$
Ra	Rayleigh number, $(Gr \times Pr)$
Re	Reynolds number for the fluid, $\bar{u}h/\nu$
Ri	Richardson number, $\left(\frac{Gr}{Re^2}\right)$
T_w	constant bottom wall temperature, °C
T_∞	constant ambient temperature, °C
$\hat{t}$	dimensional time
t	nondimensional time
$\hat{u}, \hat{v}$	dimensional velocity components along (x, y) axes, m/s
u, v	dimensionless velocity components along (x, y) axes
$\bar{u}$	inlet mean velocity, m/s
U_{max}	maximum velocity in normal directions, m/s
$\hat{x}, \hat{y}$	dimensional Cartesian co-ordinates along and normal to the plate, m
x, y	dimensionless Cartesian co-ordinates $(\hat{x}, \hat{y})/h$
x_1	reattachment length

Greek symbols

α	thermal diffusivity, m^2/s
β	coefficient of thermal expansion
ΔT	temperature difference, $T_w - T_\infty$, °C
ε	convergence criterion
η	similarity variable
ν	kinematic viscosity, m^2/s
ρ	density, kg/m^3
ν	kinematic viscosity, m^2/s
ψ	dimensionless stream function
ω	dimensionless vorticity

Subscripts

w	wall
∞	ambient condition

asymmetric heating channel with a series of conductive fins. They arranged identical fins on the hotter wall at equal streamwise spaces so that a periodic flow character prevails in the fully developed region. They found that in addition to recirculating flow at the rear of each fin, a secondary recirculating vortex appears near the colder wall when the heating of hotter wall is sufficiently intense. Their study was governed by Grashof number, Reynolds number, and the geometric parameters such as fin pitch, fin height and the inclination angle of channel. Hong et al. [4] have presented results for a two-dimensional laminar flow in an inclined duct with a backward-facing step for both buoyancy-assisting and the buoyancy opposing flow conditions. In their study the wall downstream of the step is maintained at a uniform flux, while straight wall that forms the other side of the duct is maintained at a constant temperature equivalent to the inlet fluid temperature and the wall upstream of step is considered as adiabatic surface. They have reported the effect of inclination angle and Prandtl number on velocity and temperature distributions.

Nesreddine et al. [5] have numerically investigated the laminar upward and downward flows with mixed convection in a thin vertical tube with a short uniformly heated section. They performed calculations for $Pr = 0.7$ corresponding to low Reynolds numbers from 20 to 500 and a wide range of Grashof numbers. Their results reveal that axial diffusion plays a significant role in preheating the fluid upstream from the entrance of the heat transfer region for both aiding and opposing buoyancy, with a stronger effect for latter, and can lead to flow reversal. Roy Choudhury and Jaluria [6] have investigated the flow and heat transfer associated with the convective cooling of a heated cylinder moving in a channel with buoyancy and pressure-induced flow. They have considered transport mechanisms which arise due to material motion, forced flow, and buoyancy. They observed that the flow opposes the movement of rod, either due to pressure-induced flow or due to buoyancy. A recirculating region arises near the rod surface and this recirculation region plays a major role in the heat transfer and thus affects the resulting temperature decay in the moving rod. Kim et al. [7]

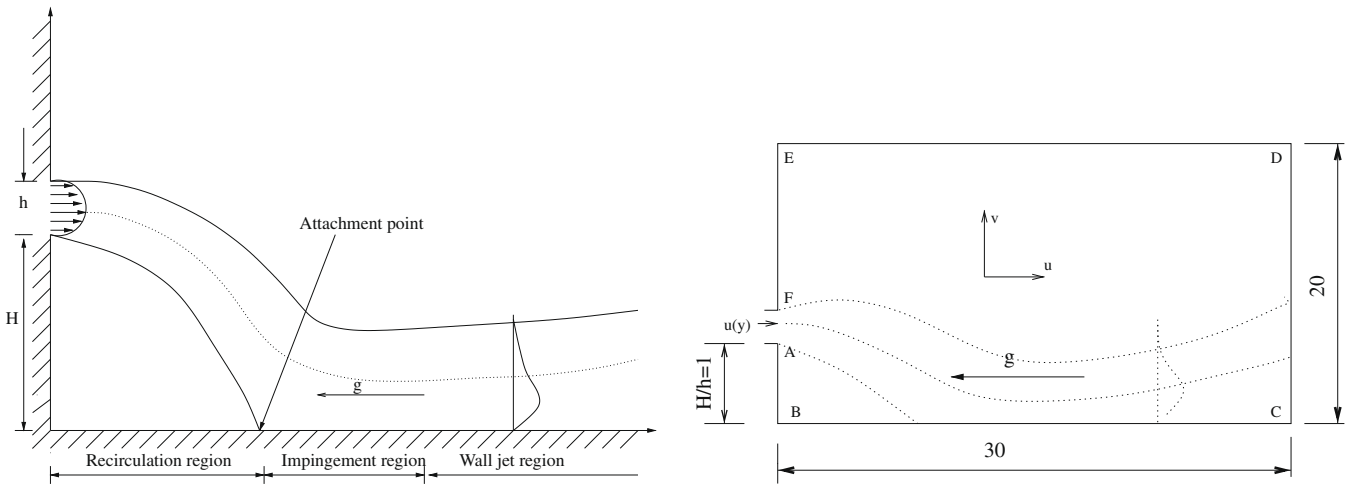

(a) Schematic diagram of the problem (b) Computational domain

Fig. 1. Buoyant assisting mixed convection in laminar offset jet flow.

have made a comprehensive analysis of the flow and heat transfer characteristics of mixed convection in a channel with rectangular blocks attached on one channel wall. They have presented details of the flow and thermal fields, for Reynolds numbers ranging from 100 to 1500 and Grashof numbers in the range of 0 to 2×10^6. Their study covers two representative cases, i.e a horizontally oriented channel and a vertically oriented channel. They traced behavior of local Nusselt number along the block surfaces and depicted the trend of maximum chip temperature vs *Re*.

Wu and Perng [8] made an analysis of the unsteady flow and heat transfer characteristics of mixed convection in a vertical block-heated channel with and without installing an inclined plate above upstream block. Their parameter studies include the inclined plate angle, Reynolds number (ranging from 260 to 530), and Grashof number (in the range of $0-3.2 \times 10^6$) on heat transfer performance. They reported that the installation of an inclined plate in the vertical block-heated channel can effectively augment the block's heat transfer performance in the channel. Lin et al. [9] presented results for laminar, buoyancy-assisting, two-dimensional flow in a vertical duct with a backward-facing step. Their study examines a wide range of inlet flow and wall temperature conditions to cover the domain from pure forced convective flow, where the buoyancy force effects were not present, to the inlet starved convective flow where the buoyancy force effects are significant and where the average inlet velocity is smaller than the corresponding natural convective value. They observed that the buoyancy induced flow decreases the reattachment length and pushes the recirculating region away from heated wall. Gau et al. [10] studied experimentally buoyancy-assisted convection flow and heat transfer processes in a heated vertical channel where the buoyancy parameter $\frac{Gr}{Re^2}$ is relatively very large. They visualized a reversed flow, which occurs initially near the channel exit for the case when $\frac{Gr}{Re^2}$ is greater than a threshold value. They observed that the reversed flow occurs near downstream of the duct and gradually propagates upstream as the buoyancy parameter $\frac{Gr}{Re^2}$ increases. They measured the penetration depth of the reversed flow and compared with prediction based on simple model. They also measured local and average Nusselt numbers. Cheng et al. [11] made predictions of buoyancy-assisted flow reversal and convective heat transfer in the entrance region of a vertical rectangular duct. They investigated physical situations which include cases with various asymmetric heating conditions over a wide range of parameters and they presented an analytical solutions for the fully developed flows.

Glauert [12] has defined a plane wall jet as a stream of fluid blown tangential along a plane wall. Similarity solution for plane wall jet as well as radial wall jet for both laminar and turbulent cases were presented with the introduction of Glauert constant '*F*'. Schwarz and Caswell [13] have investigated the heat transfer characteristics of a two-dimensional laminar incompressible wall jet. They have found exact solutions for both constant wall temperature and constant heat flux cases. In addition, they have solved for variable starting length of the heated section at constant wall temperature. The solution was derived with the plate and jet regimes as non-conjugated.

Angirasa [14] has studied a laminar buoyant wall jet and reported the effect of velocity and the width of the jet during convective heat transfer from the vertical surface. Sahoo and Sharif [15] have investigated the flow and heat transfer characteristics in the jet impingement cooling of a constant heat flux surface numerically. Computations are done for vertically downward directed two-dimensional confined slot jets impinging on a constant heat flux surface at the bottom. The principal objective of this study is to investigate the associated heat transfer process in the mixed convection regime. Kanna and Das [16] have studied the conjugate laminar plane wall jet and reported a closed form solution for interface temperature, local Nusselt number and average Nusselt number. Later, Kanna and Das [17] have numerically simulated two-dimensional transient laminar incompressible offset jet flows to gain insight into convective recirculation and flow process induced by an offset jet. They described the behavior of the jet with respect to offset ratio (OR) and Reynolds number. They found that the reattachment length was dependent on both *Re* and *OR* for the range considered. The governing equation is solved by ADI (alternating direct implicit) method and clustered cartesian grids are used for the computations. In a later study, Kanna and Das [18] have also reported the conjugate heat transfer of a laminar offset jet.

Though a considerable amount of study is carried out on laminar plane wall jet flow, buoyancy-assisted laminar offset jet is not reported by any researcher. This type of flow situation occurs in electronics cooling, refrigerated air curtain, paper industry, electrical motor cooling, etc. In an electronic equipment, a fan situated in one compartment blows air through slots to cool heated components mounted on vertical surfaces in another compartment [14]. The velocities are low, and laminar flows may prevail. In order to understand the basic physics of the interaction between the forced jet flow and the natural convection flow that arises due to the temperature difference between the wall and the ambient, a numerical study has been carried out for laminar flows.

2. Problem definition

A two-dimensional, incompressible, mixed convection in a laminar offset jet flow is considered for the study. The schematic diagram of the physical problem and the boundary conditions of the problem under consideration are shown in Fig. 1a and b, respectively. A surface of length 30 times the height of the slot in streamwise direction is maintained at a temperature T_w, which is higher than the ambient temperature T_∞. The velocity distribution in the jet is taken as parabolic and its temperature is same as the ambient temperature. The width of the jet is h which is equal to the slot height. Except the jet slot AF, the wall BE is assumed to be adiabatic, as shown in Fig. 1b.

2.1. Governing equations

The unsteady stream function-vorticity equations governing the incompressible mixed convection laminar flow in non-dimensional form are

Vorticity transport equation:

$$\frac{\partial \omega}{\partial t} + \frac{\partial (u\omega)}{\partial x} + \frac{\partial (v\omega)}{\partial y} = \frac{1}{Re}(\nabla^2 \omega) - \frac{Gr}{Re^2}\frac{\partial \theta}{\partial y} \tag{1}$$

where Reynolds number $Re = \frac{\bar{u}h}{\nu}$

The vorticity ω is given by

$$\omega = \frac{\partial v}{\partial x} - \frac{\partial u}{\partial y} \tag{2}$$

The relations between velocities and stream function are

$$u = \frac{\partial \psi}{\partial y}, v = -\frac{\partial \psi}{\partial x} \tag{3}$$

Poisson equation for the stream function,

$$\frac{\partial^2 \psi}{\partial x^2} + \frac{\partial^2 \psi}{\partial y^2} = -\omega \tag{4}$$

Energy equation,

$$\frac{\partial \theta}{\partial t} + \frac{\partial (u\theta)}{\partial x} + \frac{\partial (v\theta)}{\partial y} = \frac{1}{RePr}\nabla^2 \theta \tag{5}$$

The following non-dimensional variables used for Eqs. (1)–(5) are

$$x=\frac{\hat{x}}{h}, y=\frac{\hat{y}}{h}, u=\frac{\hat{u}}{\bar{u}}, v=\frac{\hat{v}}{\bar{u}}, \psi=\frac{\hat{\psi}}{h\bar{u}}, \omega=\frac{h\hat{\omega}}{\bar{u}},$$
$$\theta=\frac{T-T_\infty}{T_w-T_\infty}, t=\frac{\hat{t}}{(h/\bar{u})}$$

with the overbar indicating a dimensional variable and $\bar{u}, h$ denoting the average jet velocity at nozzle exit and the jet width, respectively.

The boundary conditions needed for the numerical simulation have been prescribed. The following dimensionless conditions have been enforced as shown in Fig. 1b. The inlet slot height is assumed as 0.05 m.

At the jet inlet, along AF (Fig. 1b),

$$u(y)=120y-2400y^2; \omega(y)=4800y-120; \quad \psi(y)=60y^2-800y^3 \tag{6a}$$

Along FE, AB and BC, due to no-slip condition,

$$u=v=0 \tag{6b}$$

Along ED,

$$\frac{\partial u}{\partial y}=0 \text{ and } \frac{\partial v}{\partial y}=0 \tag{6c}$$

At downstream boundary the condition of zero first-derivative has been applied for velocity components. This condition implies that the flow has reached a developed condition. Thus, at (DC),

$$\frac{\partial u}{\partial x}=\frac{\partial v}{\partial x}=0 \tag{6d}$$

Similar type of boundary conditions have been used by Gu [19] and Al-Sanea [20,21]. Details of the discretization of this particular boundary condition is given in Kanna and Das [22].

Thom's vorticity condition has been used to obtain the wall vorticity as given below.

$$\omega_w=-\frac{2(\psi_{w+1}-\psi_w)}{(\Delta n)^2} \tag{7}$$

where Δn is the grid space normal to the wall.

At the bottom wall and the left side wall, constant stream lines are assumed based on inlet flow. At the outlet in the downstream direction, stream-wise gradients are assumed to be zero. At the entrainment boundary, normal velocity gradient is zero [23]. The detailed boundary conditions are given below (Fig. 1b).

$$\text{at AF, } u(y)=120y-2400y^2; \psi(y)=60y^2-800.00y^3; \quad \omega(y)=4800y-120; \theta=0 \tag{8a}$$

$$\text{along FE, } u=v=0; \psi=0.050; \omega=-\frac{2\psi_w-2\psi_{w+1}}{\Delta x^2}; \frac{\partial\theta}{\partial x}=0 \tag{8b}$$

$$\text{along AB, } u=v=0; \psi=0.0; \omega=-\frac{2\psi_{w+1}}{\Delta x^2}; \frac{\partial\theta}{\partial x}=0 \tag{8c}$$

$$\text{along BC, } u=v=0; \psi=0; \omega=-\frac{2\psi_{w+1}}{\Delta y^2}; \theta=1.0 \tag{8d}$$

$$\text{along CD, } \frac{\partial u}{\partial x}=0; \frac{\partial v}{\partial x}=0; \frac{\partial\theta}{\partial x}=0; \frac{\partial\omega}{\partial x}=0 \tag{8e}$$

$$\text{along DE, } \frac{\partial v}{\partial y}=0; \theta=0 \tag{8f}$$

3. Numerical procedure

The computational domain considered here is clustered cartesian grids. The details of constructing the grids can be found from Kanna and Das [16]. The unsteady vorticity transport Eq. (1) in time is solved by alternate direction implicit scheme (ADI). The central differencing scheme is followed for the convective as well as the diffusive, buoyancy terms. It is first order accurate in time and second order accurate in space $O(\Delta t, \Delta x^2, \Delta y^2)$, and is unconditionally stable. The Poisson Eq. (4) is solved explicitly by five point Gauss–Seidel method. Constant time step of 0.001 is used for the entire calculation. The maximum vorticity error behavior as by Roache [24] is

$$\sum_{i,j=1}^{i_{max},j_{max}} |(\omega_{i,j}^{t+\Delta t}-\omega_{i,j}^{t})| < \varepsilon \tag{9}$$

The convergence criteria for temperature is given by:

$$\sum_{i,j=1}^{i_{max},j_{max}} (\theta_{i,j}^{t+\Delta t}-\theta_{i,j}^{t}) < \varepsilon \tag{10}$$

At steady-state, both the errors reach the asymptotic behavior. Steady-state is achieved when the sum of vorticity error and the temperature error are reduced to the convergence criterion.

4. Grid independence study

The computational domain used has a size of 30 times the slot height in downstream direction and 20 times slot height in normal direction. A series of grid independence study has been carried out to find the optimum grid points in both the directions. The following grid systems were considered 61×61, 65×65, 72×72, 84×84, 96×96, 105×105. It has been found that the variation of reattachment length with respect to the grid numbers at 96×96 compared to 105×105 is 0.06% which is less than 1% as shown in Fig. 2. It is concluded that the grid refinement level 5 (96×96) will be sufficient for the entire calculations. Fig. 3 shows the typical grids for the computations.

5. Validation of the code

The code developed by Kanna [25] based on the stream function-vorticity approach following ADI scheme has been tested for various problems like lid-driven cavity flow, backward-facing step flow, wall jet flow, offset jet flow, wall jet flow over backward-facing step flow. The same code has been modified to include the natural convection leading to a mixed convection flow problem.

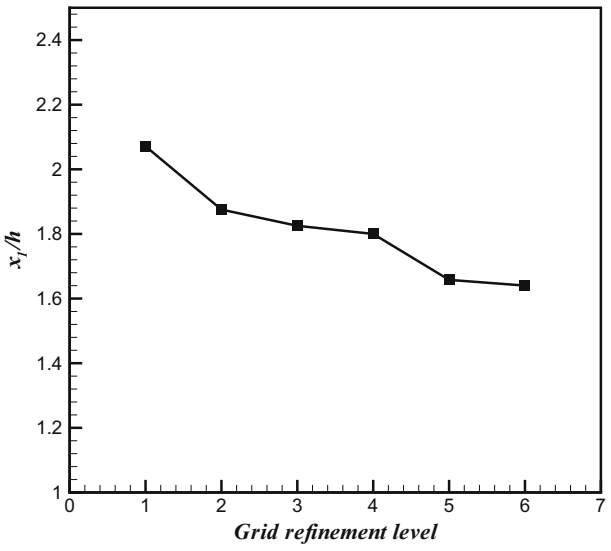

Fig. 2. Grid independence study: $Re=500$, $Pr=0.71$, $Gr=10^4$.

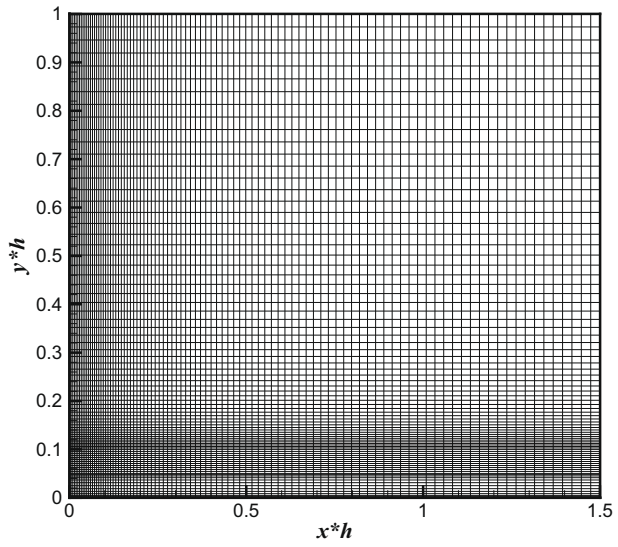

Fig. 3. Typical clustered grids used for the computations.

Angirasa [14] validated buoyant wall jet computation by comparing natural convection results of Churchill and Chu [26]. Here the buoyancy-assisting offset jet flow code is validated with $Gr = 0$ case in wall jet region. The flow becomes forced convection heat transfer for $Gr = 0$. The computed velocity and temperature profiles are compared with the available experimental and similarity solutions. The u velocity similarity profiles for different downstream locations are compared (Fig. 4a) with similarity solution of Glauert [12] and the experimental results of Quintana et al. [27]. The computed temperature similarity profile is compared (Fig. 4b) with similarity solution in a similar way as represented by Seidel [28]. It is observed that at different downstream locations good agreement amongst them has been obtained.

6. Results and discussion

The computations are performed for a range of Gr and Re where Pr is kept constant at 0.71. Accordingly $Ri = \frac{Gr}{Re^2}$ varies in a wide range. The range for Gr is 10^3–10^7 and $Re = 300$–600. So the minimum and maximum Ri are 0.0028 and 111, respectively. The offset ratio (OR) is defined as the ratio of step height H to the inlet slot height h. In the present computation, OR is considered as 1.

To understand the relative importance of natural convection versus pure forced convection on offset jet flow at a given location, the parameter Gr is varied for each Re. Forced convection dominates when $\frac{Gr}{Re^2}$ is small. The natural convection effect gradually becomes significant and starts to dominate when $\frac{Gr}{Re^2}$ inceases. Fig. 5 shows the streamline, velocity vector plot and the isotherm contours for $Re = 600$ and $Pr = 0.71$. The Grashof number is gradually varied at $10^3, 10^5, 10^6$ and 10^7. The Richardson number then becomes 0.0028, 0.28, 2.8 and 27.8. When Ri is very low (0.0028), the streamline resembles that of a forced convection (Fig. 5(k)). The streamlines obtained here is similar to that reported by Kanna and Das [17]. Due to the Coanda effect, a recirculation zone is observed at the jet exit. Another recirculation is observed at the intersection of the insulated wall and the entrainment boundary which is also present for $Ri = 0.28$ (Fig. 5d). The isotherm lines are clustered near the jet exit and spread at the downstream direction (Fig. 5c) similar to the characteristics of an offset jet heat transfer. As Ri is increased to 2.8 (Fig. 5g), the recirculation eddy diminishes in size. However, the recirculation at the entrainment boundary disappears. A recirculation at the jet exit boundary is observed which increases in size with increase in $Ri = 27.8$ (Fig. 5j). The isotherms are getting even more clustered with an increase in heat transfer.

Because of the accelerated flow, the fluid is attached towards the heated wall (Fig. 6a, c and e), and that trend increases as the buoyancy (Gr) increases. Increased buoyancy will also decrease the reattachment length, reduce the size of the recirculation region as shown in Fig. 6b, d and f. The recirculation region splits into two recirculations at $Gr = 10^6$ as shown in Fig. 6f. At $Gr > 10^6$, the recirculation region disappears from the flow and the flow becomes similar to that of a wall jet flow.

The general flow characteristics in the recirculation region as affected by increasing the buoyancy force is clearly shown in Fig. 7 for Reynolds numbers 300 and 600 with $Gr = 10^3, 10^6$ and 10^7. These figures capture only a small region of the calculation domain to highlight the influence of buoyancy forces on the recirculation region. As Gr increases, the reattachment length decreases and

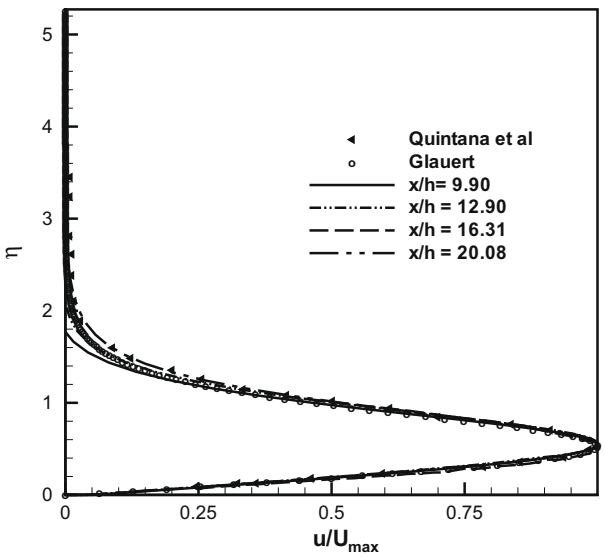

(a) Comparison of horizontal velocity profile

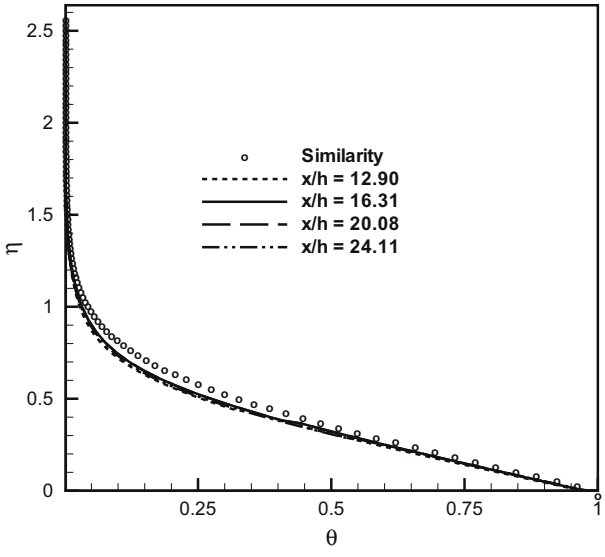

(b) Comparison of temperature profile

Fig. 4. Comparison of results with similarity solution for $Re = 500, Gr = 0.0, Pr = 1.4$.

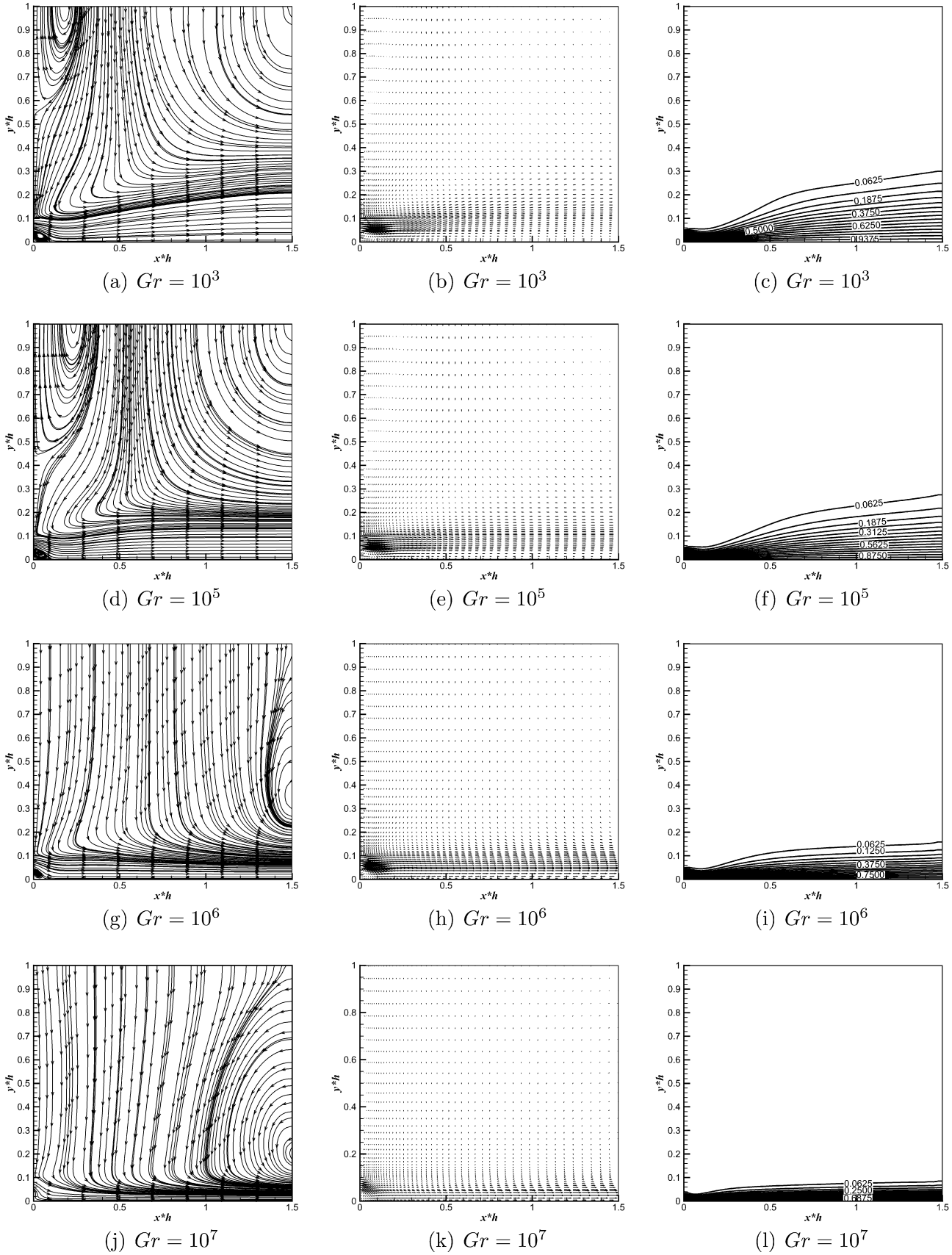

(a) $Gr = 10^3$ (b) $Gr = 10^3$ (c) $Gr = 10^3$

(d) $Gr = 10^5$ (e) $Gr = 10^5$ (f) $Gr = 10^5$

(g) $Gr = 10^6$ (h) $Gr = 10^6$ (i) $Gr = 10^6$

(j) $Gr = 10^7$ (k) $Gr = 10^7$ (l) $Gr = 10^7$

Fig. 5. Streamline (left), vector field (middle) and isotherm (right) contours for $Pr = 0.71, Re = 600$.

the size of the recirculation region decreases for a particular *Re*. This trend continues until the flow becomes similar to that of a wall jet flow, but the recirculation region moves towards the insulated wall from the heated wall at high *Gr*. An increase in the Rey-

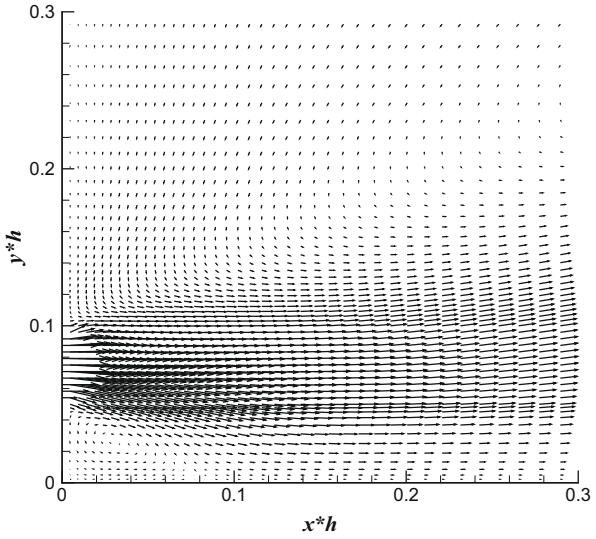

(a) $Gr = 10^3$

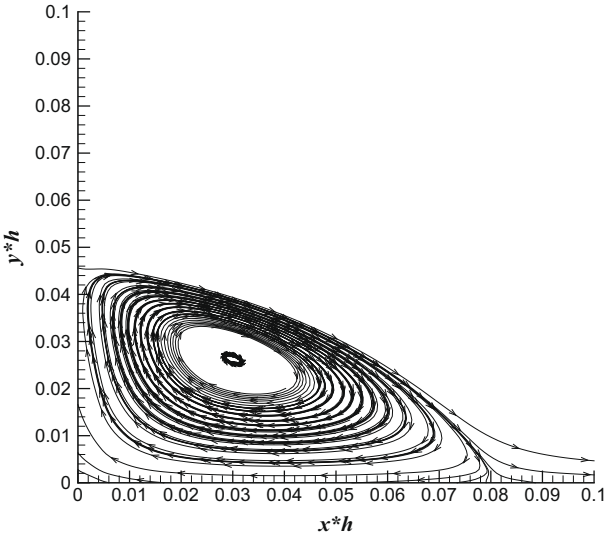

(b) $Gr = 10^3$

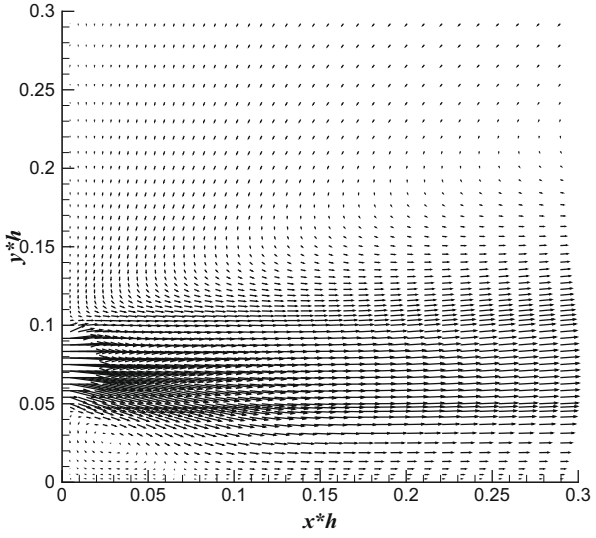

(c) $Gr = 10^5$

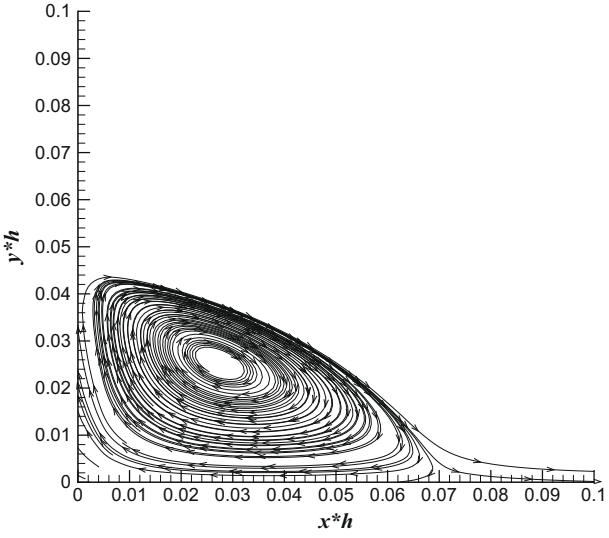

(d) $Gr = 10^5$

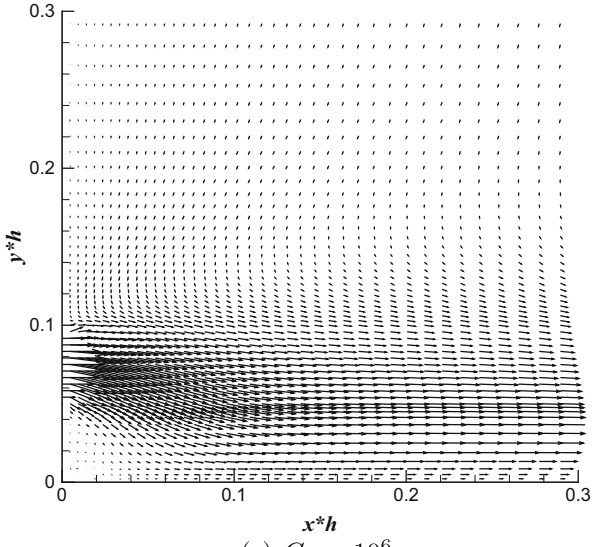

(e) $Gr = 10^6$

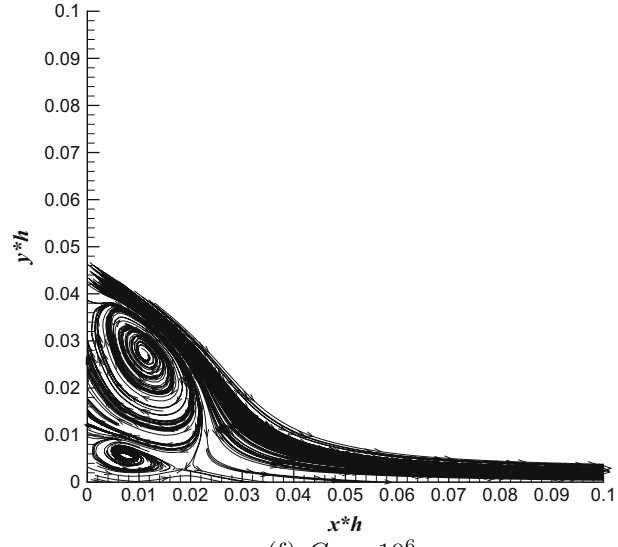

(f) $Gr = 10^6$

Fig. 6. Velocity vector (left) and recirculation eddy (right) for $Pr = 0.71, Re = 400$.

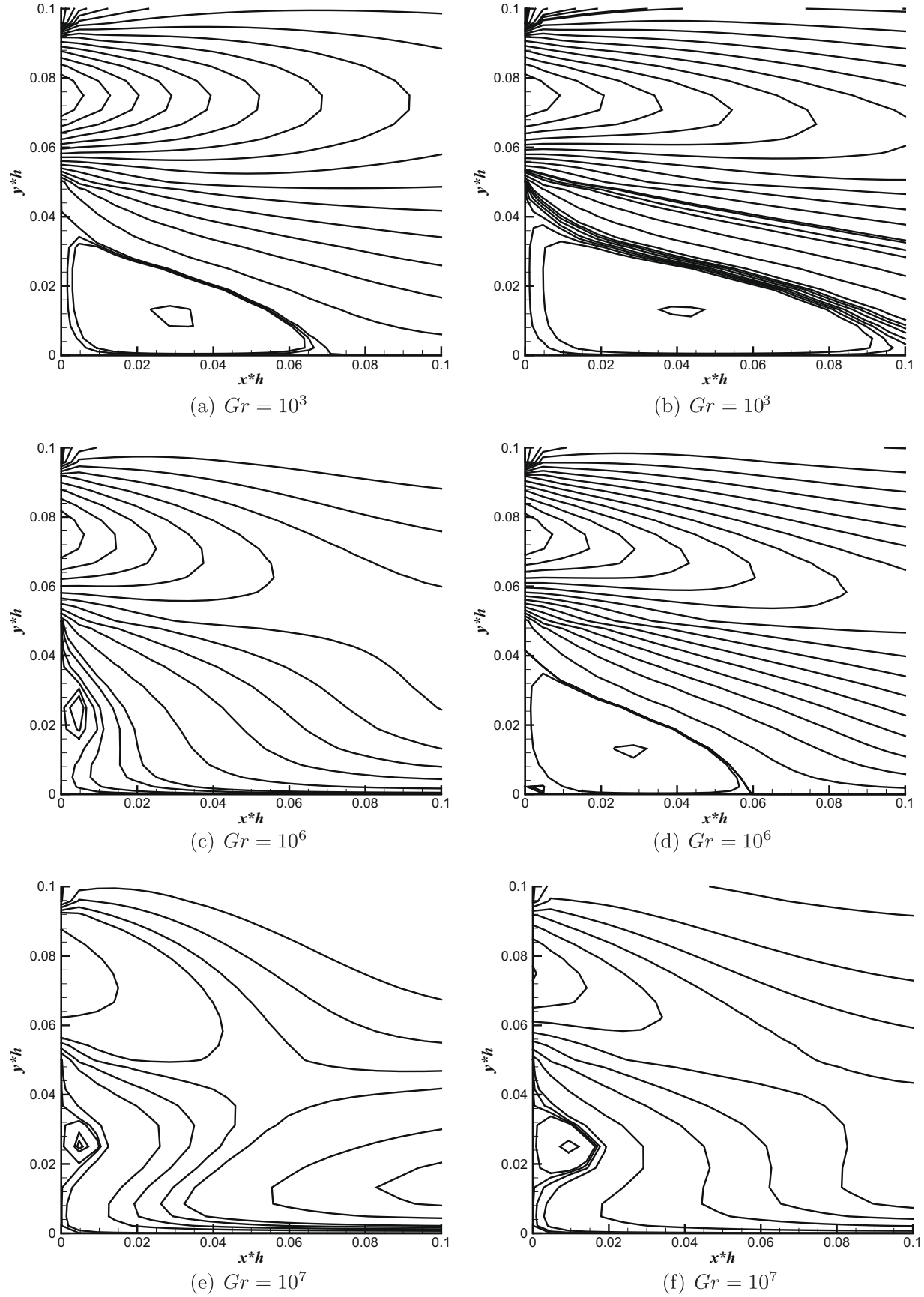

(a) $Gr = 10^3$ (b) $Gr = 10^3$

(c) $Gr = 10^6$ (d) $Gr = 10^6$

(e) $Gr = 10^7$ (f) $Gr = 10^7$

Fig. 7. Comparison of recirculation eddy for $Re = 300$ (left) and $Re = 600$ (right).

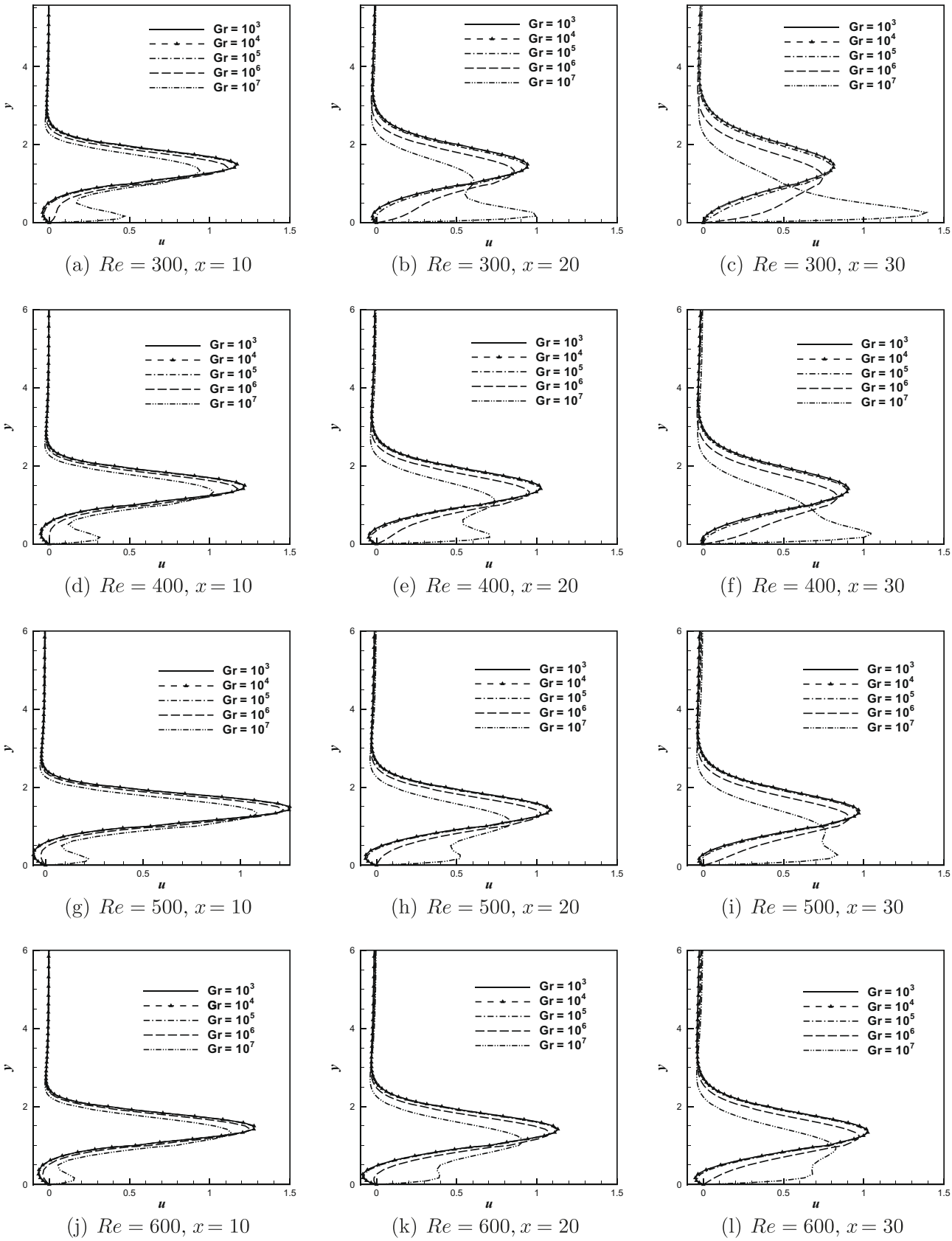

Fig. 8. *u*-Velocity component for various *Re* and *Gr* at different locations.

nolds number for a fixed *Gr* will decrease the buoyancy parameter, $\frac{Gr}{Re^2}$, and will delay the reattachment, thereby increasing the size of recirculation as shown in Fig. 7a and b. At $Gr = 10^6$, for $Re = 300$ the recirculation region moves towards the insulated wall (Fig. 7c), whereas for $Re = 600$ it still remains attached with the heated wall (Fig. 7d). It is due to the increased inertia force at high

Re. At $Gr = 10^7$, for both $Re = 300$ and 600, the recirculation moves adjacent to the insulated wall, but for $Re = 600$ the recirculation is bigger in size.

The effects of buoyancy force on the velocity distribution is presented in Fig. 8. In the Fig. 8a–c, it is observed that for $Gr = 10^3$ and 10^4, the velocity decreases in the downstream direction because of forced convection. Also to be noted is the change in the *u*-velocity profile for $Gr = 10^7$. Since this is dominated by natural convection, the maximum *u*-velocity decreases in the downstream direction. As *Re* increases to 400, (Fig. 8d–f), the effect of forced convection

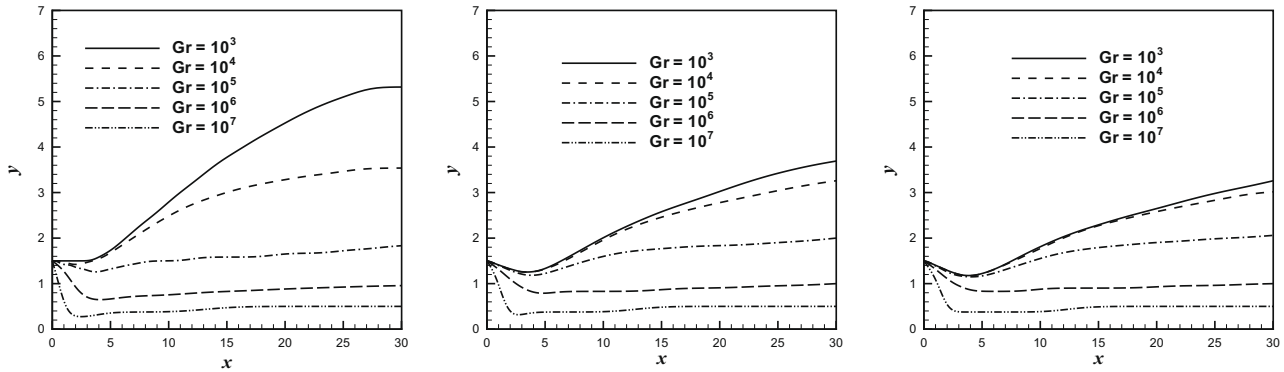

(a) $Re = 300$ (b) $Re = 500$ (c) $Re = 600$

Fig. 9. u_{max} trajectory for various *Re*.

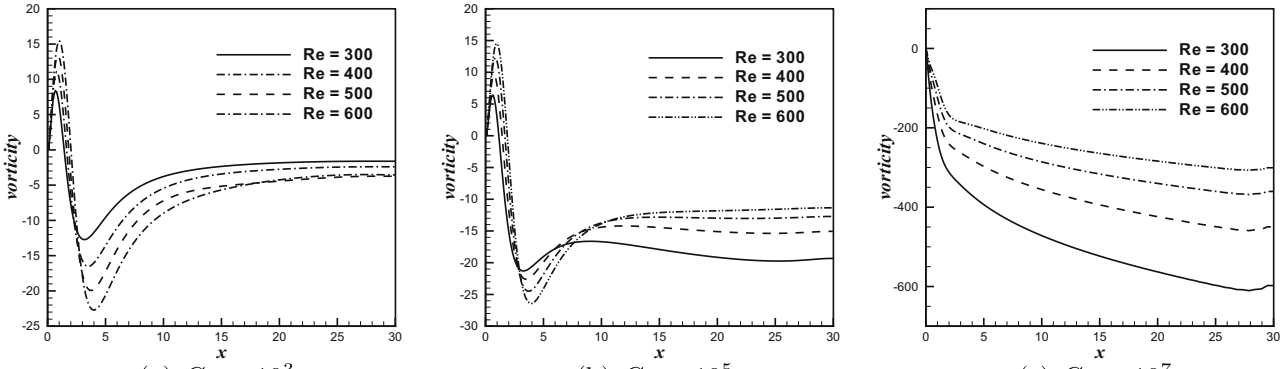

(a) $Gr = 10^3$ (b) $Gr = 10^5$ (c) $Gr = 10^7$

Fig. 10. Vorticity distribution along bottom wall.

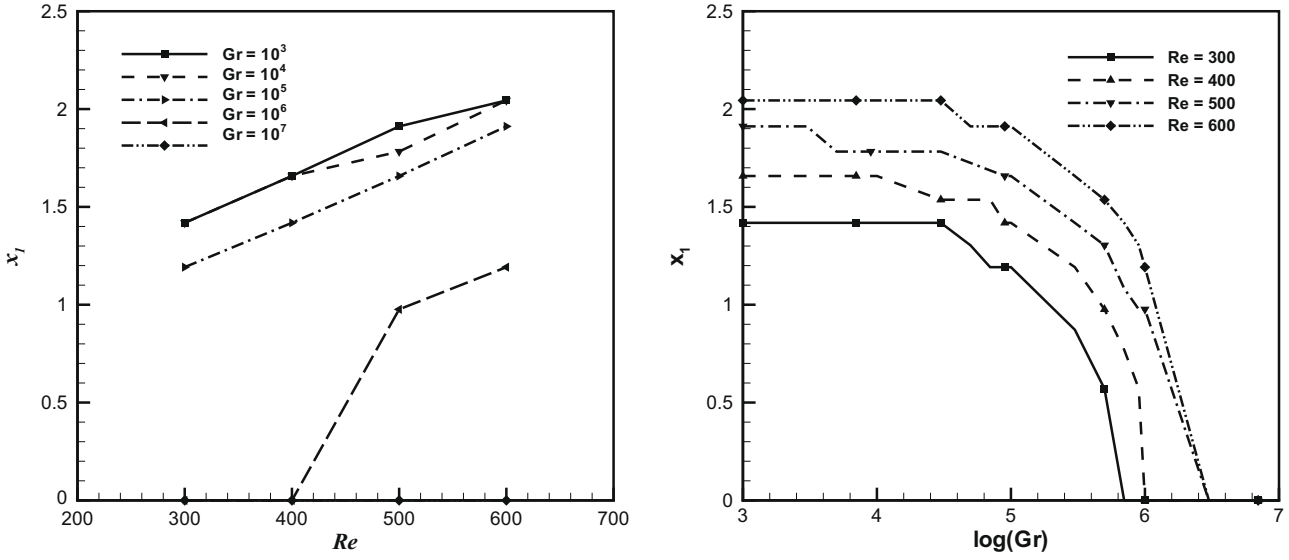

(a) variation with *Re* (b) variation with *Gr*

Fig. 11. Variation of reattachment length with *Re* and *Gr*.

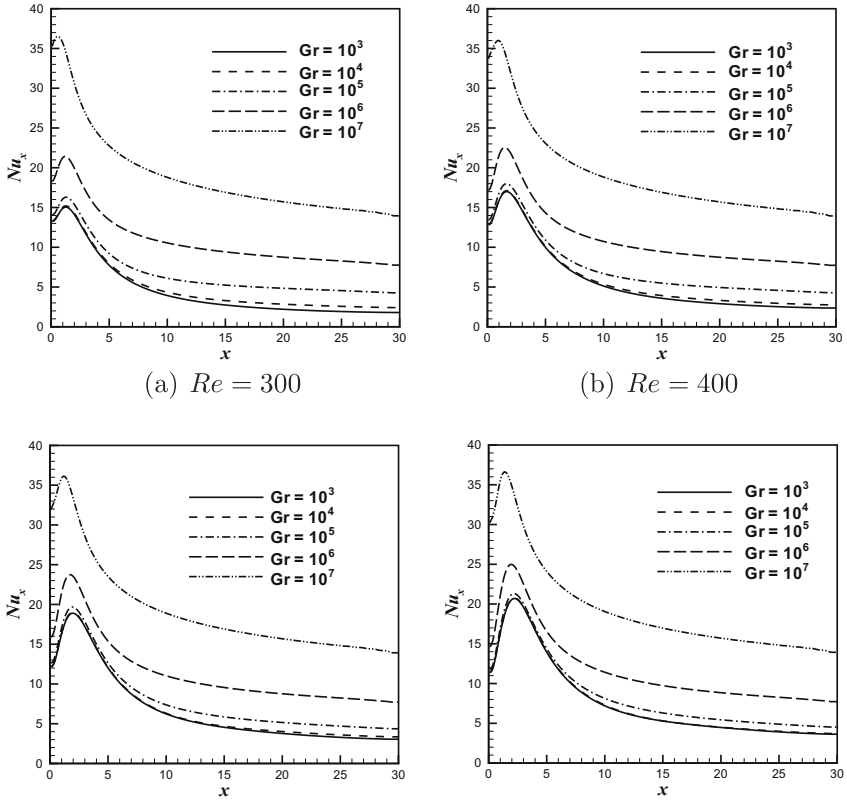

Fig. 12. Nusselt number variation with *Re*.

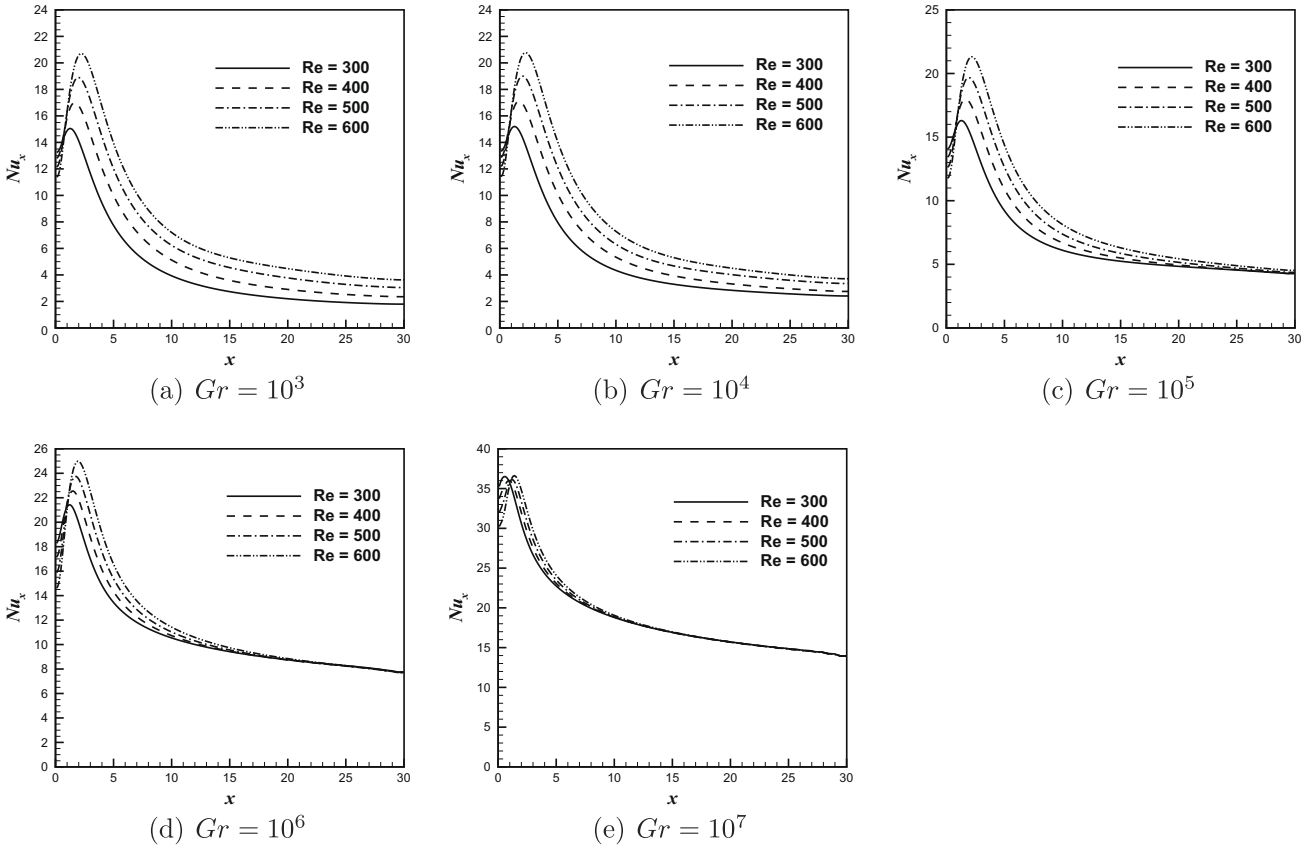

Fig. 13. Nusselt number variation with *Gr*.

Table 1
Effect of *Re* and *Gr* on maximum Nusselt number and its location

Re	*Gr*	Nu_{max}	*x*
300	10^3	15.048	1.303
300	10^4	15.198	1.303
300	10^5	16.301	1.303
300	10^6	21.427	1.192
300	10^7	36.514	0.570
400	10^3	17.001	1.657
400	10^4	17.115	1.657
400	10^5	17.991	1.657
400	10^6	22.548	1.536
400	10^7	35.998	0.976
500	10^3	18.895	1.911
500	10^4	18.999	1.911
500	10^5	19.677	1.911
500	10^6	23.743	1.782
500	10^7	36.135	1.192
600	10^3	20.699	2.180
600	10^4	20.770	2.180
600	10^5	21.312	2.180
600	10^6	24.986	1.911
600	10^7	36.620	1.418

increases and that of natural convection decreases since *Ri* is decreasing. These effects are more pronounced as *Re* is increased to 500 (Fig. 8g–i) and to 600 (Fig. 8(j)-(l)). The trajectory of maximum horizontal velocity (Fig. 9) is traced for different *Re*, varying *Gr* for each $Re = 300$, 500 and 600. It is observed that, at a particular *Re*, the U_{max} trajectory moves closer to the heated wall with increasing *Gr*.

The bottom wall vorticity distribution for different *Re* are shown in Fig. 10. From Eq. 2, the vorticity at bottom wall is equal to $-(\frac{\partial u}{\partial y})|_{y=0}$, (where $\frac{\partial v}{\partial x} = 0$) which is analogus to skin friction coefficient $\left(c_f = \frac{\mu(\frac{\partial u}{\partial y})|_{y=0}}{\frac{1}{2}\rho u^2}\right)$. For $Gr = 10^3$ (Fig. 10a), near the inlet, vorticity is having a large value and further in the downstream direction, it approaches an asymptotic value. This is a characteristics of a boundary layer flow. After reaching a high positive value (first peak), it falls rapidly and reaches a minimum value (second peak). The second peak indicates the impingement of jet on the heated wall. In Fig. 10a vorticity at the bottom wall for $Gr = 10^3$ with different *Re* is presented. This is almost similar to a pure forced convection case and bottom wall vorticity decreases with increase in *Re* even after jet impingement. With further increase in $Gr = 10^5$ (Fig. 10b), the jet turns as buoyant jet in the downstream region for low *Re*. At $Gr = 10^7$, the offset jet eventually becomes a buoyant jet and the absolute value of the bottom wall vorticity increases as *Re* increases.

The variation of the reattachment length with *Re* and *Gr* is presented in Fig. 11. The reattachment length is same for $Gr = 10^3$ and $Gr = 10^4$ except at $Re = 500$. At $Gr = 10^6$ the offset jet becomes a wall jet when *Re* becomes less than 400 (Fig. 11(a)). At $Gr = 10^7$ the offset jet essentially becomes a buoyant jet irrespective of *Re*. It is observed that, the reattachment length decreases with increase in *Gr* and simultaneously increases with increase in *Re* (Fig. 11b).

The effect of buoyancy force on the Nusselt number is illustrated in Fig. 12. The Nusselt number curves have the normal peak point downstream of the reattachment point. As mentioned earlier, $Gr = 10^3$ and $Gr = 10^4$ cases are very close to forced convection situations because the *Nu* curve almost overlap with each other for the whole *Gr* range (Fig. 12a–d). The *Nu* increases only when *Gr* is further increased to 10^5 and more. Natural convection starts to dominate at and above $Gr = 10^5$ and *Nu* increases as *Gr* increases. At Grashof numbers $10^3, 10^4$, the heat transfer (Nusselt number) varies with each *Re* (Fig. 13a–b). It can be observed in Fig. 13c–e that the variation of *Nu* with *Re* gradually diminishes and at $Gr = 10^7$, the effect of *Re* is almost insignificant. It should be noted that the peak in the Nusselt number distribution continues to occur even after the reduction in the size of the recirculation bubble ($Gr = 10^7$) as shown in Fig. 13e.

The effect of *Re* and *Gr* on maximum local Nusselt number (Nu_{max}) and its location is presented in Table 1. It is observed that maximum Nusselt number shifts to left with increase in *Gr* and to right with increase in *Re*, which is anticipated.

7. A heat transfer correlation

The numerically calculated heat transfer results were correlated for mixed convection in offset jet flow. About 100 numerical data are generated, encompassing the range of parameters $0.00278 \leqslant Ri \leqslant 111.112$ and $300 \leqslant Re \leqslant 600$. The non-dimensional length is 30 and the offset ratio is 1. It can be shown that the average Nusselt

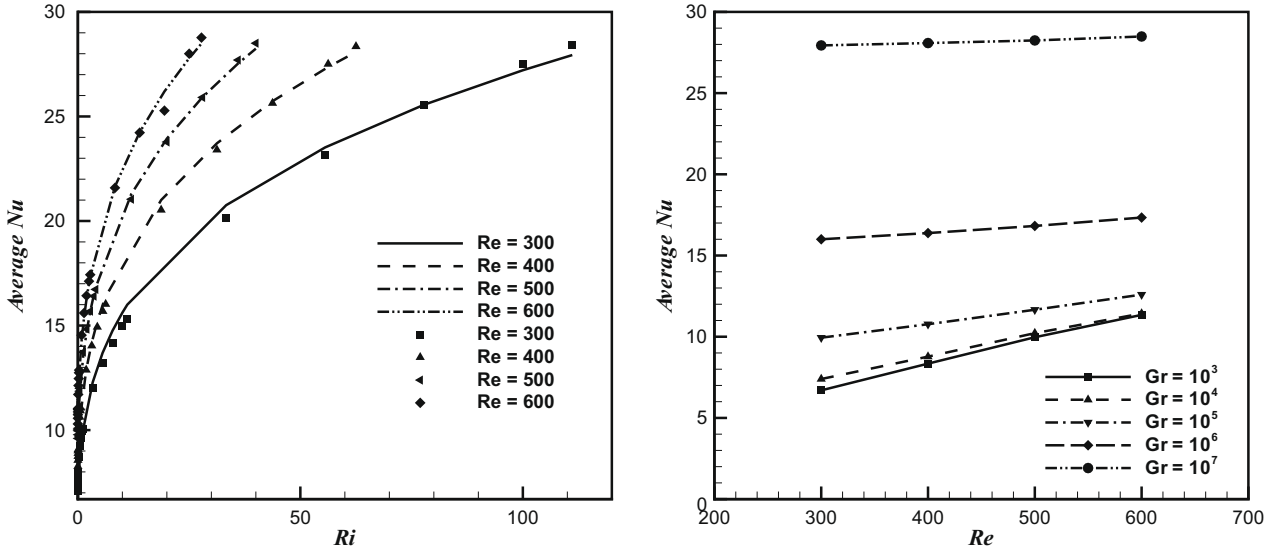

Fig. 14. Average Nusselt number variation with *Re* and *Gr*. Lines are computational results and symbols are correlation results.

number is correlated as a function of Richardson number and Reynolds number (Ri,Re) according to the following equation.

$$\overline{Nu} = 0.232(1 + 0.53Ri^{0.396})Re^{0.586} \quad (11)$$

This correlation is valid for $Pr = 0.71$ (air). Correlation results (symbols) are compared with computational results (lines) in Fig. 14. When the buoyancy becomes significant, the heat transfer parameter Nu increases with increasing Ri for the Re chosen. The results clearly indicate that buoyancy-assisted flow can enhance the heat transfer process.

8. Conclusions

The flow and heat transfer study of mixed convection flow of an offset jet has been carried out where the buoyancy is assisting the forced convection. The following conclusions may be drawn:

- A recirculation eddy is formed similar to the case of a forced convection when Ri is small (=0.0028). As Ri is increased, the size of this eddy reduces. At high Ri value (i.e. high Gr value), it disappears because of the dominance of the natural convection flow.
- With the increase of Gr, the U_{max} trajectory moves closer to the wall.
- The absolute value of the vorticity at heated wall decreases in the downstream direction for low Gr value ($= 10^3$). When Gr is increased (10^7), the absolute value of the vorticity at heated wall increases in the downstream direction.
- The local Nu number for $Gr = 10^3$ and 10^4 almost overlap with each other. A marked improvement is observed when Gr is increased to 10^6 and 10^7. At low Gr (10^3), Re is having an effect on Nu. However, at high Gr (10^7), Re does not have any significant effect on the local Nu distribution.
- An empirical correlation has been proposed to predict $\overline{Nu}$ as a function of Ri and Re for the range of $0.0028 \leqslant Ri \leqslant 111$ and $300 \leqslant Re \leqslant 600$.

Acknowledgement

The authors are thankful to the helpful and detailed comments of the reviewers.

References

[1] D.J. Tritton, Physical Fluid Dynamics, Von Norstrand Reinhold, UK, 1977. pp. 284–286.
[2] F.J. Higuera, Opposing mixed convection flow in a wall jet over a horizontal plate, J. Fluid Mech. 342 (1997) 355–375.
[3] C.H. Cheng, C.D. Luy, W.H. Hung, Buoyancy effect on the heat convection in vertical channels with fin array at low Reynolds numbers, Int. J. Heat Mass Transfer 35 (1992) 2643–2653.
[4] B. Hong, B.F. Armaly, T.S. Chen, Laminar mixed convection in a duct with a backward-facing step: the effects of inclination angle and Prandtl number, Int. J. Heat Mass Transfer 12 (1993) 3059–3067.
[5] H. Nesreddine, N. Galanis, C.T. Nguyen, Effect of axial diffusion on laminar heat transfer with low Peclet numbers in the entrance region of thin vertical tubes, Numer. Heat Transfer: Part A 33 (1998) 247–266.
[6] S. Roy Choudhury, Y. Jaluria, Cylinder moving in pressure and buoyancy induced channel flow: a numerical study of transport due to the aiding/opposing mechanisms, Numer. Heat Transfer: Part A 27 (1995) 373–393.
[7] S.Y. Kim, H.J. Jin Sung, J.M. Hyun, Mixed convection from multiple-layered boards with cross-streamwise periodic boundary conditions, Int. J. Heat Mass Transfer 35 (1992) 2941–2952.
[8] H.W. Wu, S.W. Perng, Heat transfer augmentation of mixed convection through vortex shedding from an inclined plate in a vertical channel containing heated blocks, Numer. Heat Transfer: Part A 33 (1998) 225–244.
[9] J.T. Lin, B.F. Armaly, T.S. Chen, Mixed convection in buoyancy-assisting, vertical backward-facing step flows, Int. J. Heat Mass Transfer 33 (1990) 2121–2132.
[10] C. Gau, K.A. Yih, W. Anug, Reversed flow structure and heat transfer measurements for buoyancy-assisted convection in a heated vertical duct, ASME J. Heat Transfer 114 (1992) 928–935.
[11] C.H. Cheng, C.J. Weng, W. Aung, Buoyancy-assisted flow reversal and convective heat transfer in entrance region of a vertical rectangular duct, Int. J. Heat Fluid Flow 21 (2000) 403–411.
[12] M.B. Glauert, The wall jet, J. Fluid Mech. 1 (1) (1956) 625–643.
[13] W.H. Schwarz, B. Caswell, Some heat transfer characteristics of the two-dimensional laminar incompressible wall jet, Chem. Eng. Sci. 16 (1961) 338–351.
[14] D. Angirasa, Interaction of low-velocity plane jets with buoyant convection adjacent to heated vertical surfaces, Numer. Heat Transfer: Part A 35 (1999) 67–84.
[15] D. Sahoo, M.A.R. Sharif, Numerical modeling of slot-jet impingement cooling of a constant heat flux surface confined by a parallel wall, Int. J. Therm. Sci. 43 (2004) 877–887.
[16] P.R. Kanna, M.K. Das, Conjugate forced convection heat transfer from a flat plate by laminar plane wall jet flow, Int. J. Heat Mass Transfer 48 (2005) 2896–2910.
[17] P.R. Kanna, M.K. Das, Numerical simulation of two-dimensional laminar incompressible offset jet flows, Int. J. Numer. Meth. Fluids 49 (2005) 434–464.
[18] P.R. Kanna, M.K. Das, Conjugate heat transfer study of two-dimensional laminar incompressible offset jet flows, Numer. Heat Transfer: Part A 48 (7) (2005) 671–691.
[19] R. Gu, Modelling two-dimensional turbulent offset jets, J. Hydraulic Eng. 122 (11) (1996) 617–624.
[20] S.A. Al-Sanea, Convection regimes and heat transfer characteristics along a continuously moving heated vertical plate, Int. J. Heat Fluid Flow 24 (2003) 888–901.
[21] S.A. Al-Sanea, Mixed convection heat transfer along a continously moving heated vertical plate with suction or injection, Int. J. Heat Mass Transfer 47 (2004) 1445–1465.
[22] P.R. Kanna, M.K. Das, A short note on the entrainment and exit boundary conditions, Int. J. Numer. Meth. Fluids 50 (8) (2006) 973–985.
[23] S.H. Kang, R. Greif, Flow and heat transfer to a circular cylinder with a hot impinging air jet, Int. J. Heat Mass Transfer 35 (9) (1992) 2173–2183.
[24] P.J. Roache, Fundamentals of Computational Fluid Dynamics, Hermosa, USA, 1998 (Chapter 3).
[25] P.R. Kanna, Numerical Study of Flow and Conjugate Heat Transfer in Plane Laminar Offset Wall Jets. Ph.D. Thesis, Department of Mechanical Engineering. Indian Institute of Technology Guwahati, India, 2005.
[26] S.W. Churchill, H.H.S. Chu, Correlating equations for laminar and turbulent free convection from a vertical plate, Int. J. Heat Mass Transfer 18 (1975) 1323–1329.
[27] D.L. Quintana, M. Amitay, A. Ortega, I.J. Wygnanski, Heat transfer in the forced laminar wall jet, J. Heat Transfer 119 (1997) 451–459.
[28] J. Seidel. Numerical Investigations of Forced Laminar and Turbulent Wall Jets Over a Heated Surface. Ph.D. Thesis, Faculty of the department of Aerospace and Mechanical Engineering. The Graduate College, The University of Arizona, Tucson, USA, 2001.